Inorganic Chemistry

pubs.acs.org/IC

Article

Deep-Tissue Temperature Sensing Realized in $BaY_2O_4:Yb^{3+}/Er^{3+}$ with Ultrahigh Sensitivity and Extremely Intense Red Upconversion Luminescence

Guotao Xiang,* Xiaotong Liu, Qing Xia, Sha Jiang, Xianju Zhou, Li Li, Ye Jin, Li Ma, Xiaojun Wang,* and Jiahua Zhang*

Cite This: *Inorg. Chem.* 2020, 59, 11054−11060

Read Online

ACCESS | Metrics & More | Article Recommendations | Supporting Information

ABSTRACT: In this paper, $BaY_2O_4:Yb^{3+}/Er^{3+}$, a high efficient red upconversion (UC) material, is first utilized as an optical thermometer in the biological window, accomplished through the fluorescence intensity ratio (FIR) of thermally coupled Stark sublevels of $^4F_{9/2}$ ($FIR_{(654/663)}$). The maximum absolute sensitivity of $FIR_{(654/663)}$) is 0.19% K^{-1} at 298 K, which is much higher than most previous reports about FIR-based temperature sensors located in the biological windows. More importantly, the groove of $FIR_{(654/663)}$ for thermometry is nicely located in the physiological temperature range, indicating its potential thermometry application value in biomedicine. Furthermore, a simply *ex vivo* experiment is implemented to evaluate the penetration depth of the red emission in biological tissues, revealing that a detection depth of 6 mm can be achieved without any effect on the FIR values of I_{654} to I_{663}. Beyond that, the temperature sensing behaviors of the thermally coupled levels $^2H_{11/2}$ and $^4S_{3/2}$ ($FIR_{(523/550)}$) are also investigated in detail. In the studied temperature range, the absolute sensitivity of $FIR_{(523/550)}$ monotonously increases with the rising temperature and reaches its maximum value 0.31% K^{-1} at 573 K. All the results imply that $BaY_2O_4:Yb^{3+}/Er^{3+}$ is a promising candidate for deep-tissue optical thermometry with high sensitivity.

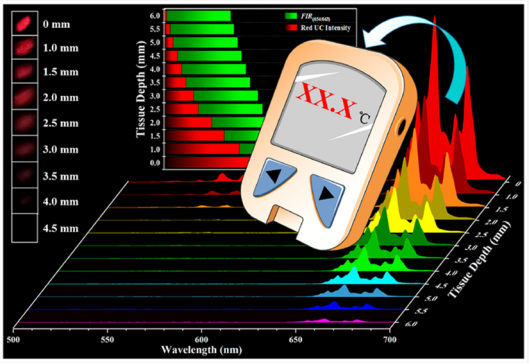

INTRODUCTION

Temperature, a very vital physical parameter, plays a crucial role in all walks of life, for instance, industrial productions, scientific studies, biomedicine, etc. Therefore, rapid and accurate thermometry is essential in practical application. Nevertheless, conventional contact thermometry, such as thermometers and thermocouples, which are based on liquid or metal expansion, are unsuitable to be utilized in some harsh and extreme environments, such as high voltage conditions, strong corrosive environments, subcutaneous circumstances, and so on.[1−12] Up to now, numerous efforts have been made to develop new kinds of noncontact optical temperature sensing techniques for the aim of solving this problem.[13−24] Generally speaking, fluorescence lifetime, fluorescence intensity, and fluorescence intensity ratio (FIR) are all highly sensitive to temperature, making them fit for optical thermometry.[25] However, utilizing fluorescence lifetime or intensity to determine temperature is strongly dependent on excitation source, optoelectronic system, background noise, and other factors, resulting in difficulties to guarantee precision and repeatability for temperature measurement. Alternatively, the optical thermometer based on FIR technology between two thermally coupled energy levels is regarded as a promising approach for temperature determination, due to its excellent antijamming capability and high detection precision as well as the rapid response ability.[26]

Particularly, the FIR thermometry based on trivalent lanthanide ions doped upconversion (UC) phosphors have received extensive interest because of the potential application as a temperature sensor *in vivo*.[27−35] Typically, in order to achieve efficient UC emission and accurate temperature measurement, erbium ion Er^{3+} with abundant ladder-like arranged energy levels, is often selected as the activator along with Yb^{3+} as the sensitizer due to its large absorption cross section around 980 nm and efficient energy transfer (ET) to Er^{3+}.[36−39] As a result, Er^{3+} could usually generate intense green UC emission derived from $^2H_{11/2} \rightarrow {}^4I_{15/2}$ and $^4S_{3/2} \rightarrow {}^4I_{15/2}$ transitions under the excitation of 980 nm wavelength. Subsequently, the optical temperature sensing can be realized based on the FIR between the thermally coupled levels

Received: May 26, 2020
Published: July 17, 2020

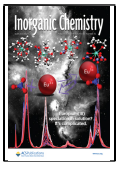

https://dx.doi.org/10.1021/acs.inorgchem.0c01543
Inorg. Chem. 2020, 59, 11054−11060

(TCLs) $^2H_{11/2}$ and $^4S_{3/2}$.[40,41] However, its practical application is greatly limited by the strong absorption for green light in the biological tissues. To date, the researches about FIR-based temperature sensors located in the biological windows (FIR-BW) have been widely carried out.[42−44] Nevertheless, the sensitivity of the FIR-BW still need to be improved to meet the requirements of photobiological applications.

Herein, BaY_2O_4:Yb^{3+}/Er^{3+} with strong red UC emission is first employed as temperature sensing probe operating in the biological window, realized by the FIR of thermally coupled Stark sublevels of $^4F_{9/2}$ ($FIR_{(654/663)}$). The absolute sensitivity of $FIR_{(654/663)}$) is much higher than the most previous reports concerned FIR-BW. Moreover, an *ex vivo* experiment is carried out to assess the penetration depth of the red emission in biological tissues, revealing that a detection depth of 6 mm can be obtained without any effect on the FIR values of I_{654} to I_{663}. Beyond that, the temperature sensing behaviors of $^2H_{11/2}$ and $^4S_{3/2}$ level are also investigated in detail. All the results propose that BaY_2O_4:Yb^{3+}/Er^{3+} owns the potential deep-tissue thermometry application value with ultrahigh sensitivity.

EXPERIMENTAL SECTION

Sample Preparation. BaY_2O_4:10% Yb^{3+}/5% Er^{3+} powder is prepared by a conventional high temperature solid state method. Typically, Y_2O_3 (99.99%), Yb_2O_3 (99.99%), Er_2O_3 (99.99%), and $BaCO_3$ (analytically pure) supplied by Chongqing Chuandong Chemical (Group) Co, Ltd. are weighed in stoichiometric proportion and ground homogeneously in an agate mortar for 60 min. Then, add the mixtures into an alumina crucible and sinter them in a box furnace at 1300 °C for 6 h. Y_2O_3:10% Yb^{3+}/4% Er^{3+} is also synthesized by the high temperature solid state method at 1550 °C for 5 h with the same rare earth sesquioxides mentioned above as the starting materials.

Characterization. A Persee XD-2 diffractometer is employed to measure the powder X-ray diffraction (XRD) data. The UC spectra are recorded by a FLS920 spectrometer.

RESULTS AND DISCUSSION

Crystal Structure. The XRD patterns of the prepared BaY_2O_4 doped with 10% Yb^{3+} and 5% Er^{3+} are measured and displayed in Figure 1a. Obviously, the relative intensities and positions of the diffraction peaks are well identified with the orthorhombic phase BaY_2O_4 standard data (JCPDS 27-0044). The lattice parameters of the sample are 1.0408, 0.3456, and 1.2126 nm for *a*, *b*, and *c*, respectively. No extraneous phase emerges in the patterns, indicating that the Yb^{3+} and Er^{3+} ions are all inserted into the matrix to form a solid solution. Likewise, as shown in Figure 1b, the prepared Y_2O_3:10% Yb^{3+}/4% Er^{3+} is also proved to be a pure phase, corresponding to the cubic Y_2O_3 standard data (JCPDS 43-1036) with the lattice parameter of 1.0637 nm.

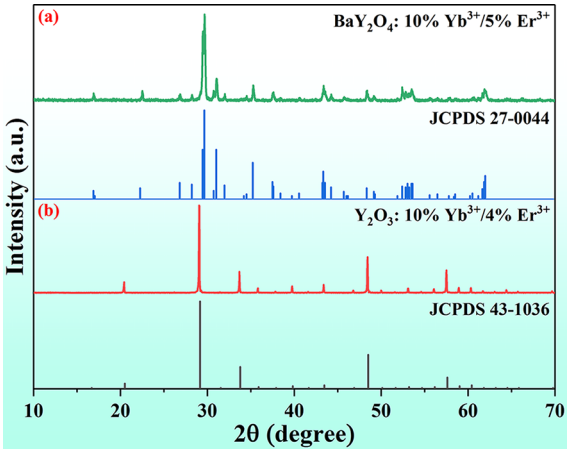

Figure 1. XRD patterns of (a) BaY_2O_4:10% Yb^{3+}/5% Er^{3+} and (b) Y_2O_3:10% Yb^{3+}/4% Er^{3+} as well as the corresponding standard XRD data.

Luminescence Properties. *UC Performance.* Figure 2a shows the UC spectrum of BaY_2O_4:10% Yb^{3+}/5% Er^{3+}, which is composed of an intense red emission band from 625 to 700 nm originating from the Er^{3+}:$^4F_{9/2}$ → $^4I_{15/2}$ transition as well as two weak green emission bands in the range of 500 nm −575 nm ascribed to the Er^{3+}:$^2H_{11/2}$/$^4S_{3/2}$ → $^4I_{15/2}$ transition. Meanwhile, the red emission band is separated into four major Stark transitions due to the crystal field effect, located at 654, 663, 674, and 680 nm, respectively. In order to assess the UC performance of the as-prepared sample, pure phase Y_2O_3, a typical oxide matrix for UC luminescence, is also synthesized with the optimal Yb^{3+} and Er^{3+} doping concentration. Obviously, as shown in Figure 2(a), BaY_2O_4:Yb^{3+}/Er^{3+} shows much stronger UC emission than Y_2O_3:Yb^{3+}/Er^{3+}, especially in the red emission region, indicating that BaY_2O_4:Yb^{3+}/Er^{3+} is a high efficient red UC material. Through integrating the intensities of the UC spectra, the green and red emission intensities of BaY_2O_4:Yb^{3+}/Er^{3+} are calculated to be 9 and 5 times stronger than those of Y_2O_3:Yb^{3+}/Er^{3+}. In addition, the energy level diagram of Yb^{3+} and Er^{3+} is presented in Figure 2b to illustrate the ET processes between them in detail. Generally, excited by 980 nm wavelength, the Yb^{3+} ions in the ground state are easily excited to $^2F_{5/2}$ level by absorbing near-infrared (NIR) photons. Next, the nonexcited Er^{3+} ions can be pumped to the green emitting levels $^2H_{11/2}$/$^4S_{3/2}$ through ET1 and ET2 processes follow by a multiphonon relaxation (MPR) process from $^4F_{7/2}$ level. Moreover, the Er^{3+} ions populated in $^4I_{11/2}$ state through ET1 process can be relaxed nonradiatively to $^4I_{13/2}$ state and then excited to $^4F_{9/2}$ state by ET3 process, resulting in the red UC emission. In addition, the $^4F_{9/2}$ state can also be populated by a MPR process from $^2H_{11/2}$/$^4S_{3/2}$ states.

Temperature Sensing Behaviors. It is universally known that the excellent UC performance and thermal coupling property of Er^{3+}:$^2H_{11/2}$ and $^4S_{3/2}$ level make them suitable for temperature sensing. However, numerous studies indicate that the optical thermometry technology based on FIR between $^2H_{11/2}$ level and $^4S_{3/2}$ level possesses poor sensitivity in the physiological temperature region because of the relative large energy gap ΔE.[45] Utilizing the FIR between a pair of thermally coupled Stark sublevels with small ΔE for temperature sensing may be a promising solution to improve the measurement sensitivity for bioapplication.[43]

Figure 3a describes the temperature dependence of red UC emission in the present sample under the excitation of 980 nm wavelength. The spectral intensities have been normalized to 1 at 663 nm. Several thermally coupled Stark transitions exist in the range of 620 nm to 720 nm, derived from the relevant energy level splitting. Notably, the FIR values of I_{654} to I_{663} are regularly increased with the increasing temperature, revealing the availability for temperature sensing.[43] Four Lorentz functions are used to fit the red UC spectra as shown in Figure S1, from which the integral intensities of I_{654} and I_{663} are calculated. According to the Boltzmann distribution law, the FIR between two thermally coupled energy levels can be expressed as follows:

https://dx.doi.org/10.1021/acs.inorgchem.0c01543
Inorg. Chem. 2020, 59, 11054−11060

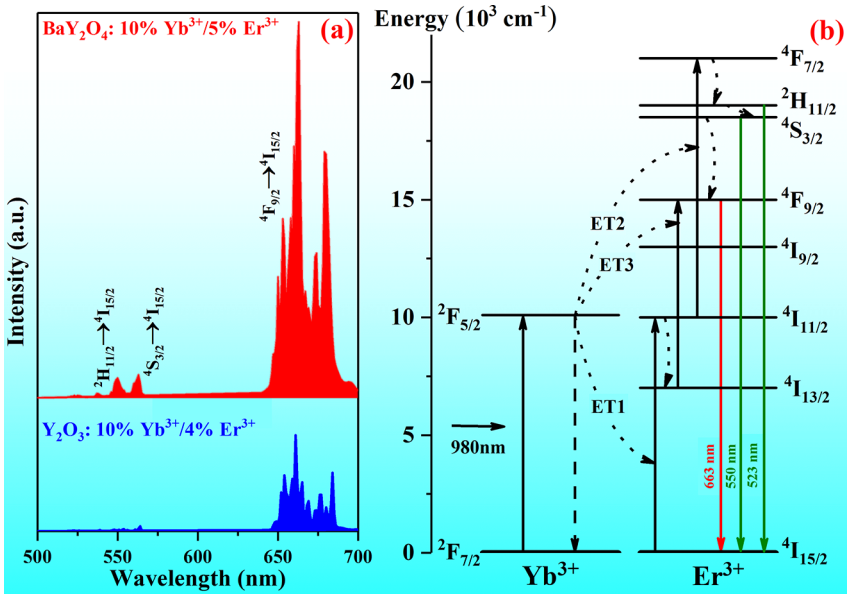

Figure 2. (a) UC spectra of BaY_2O_4:10% Yb^{3+}/5% Er^{3+} and Y_2O_3:10% Yb^{3+}/4% Er^{3+}. (b) Energy levels and possible ET processes.

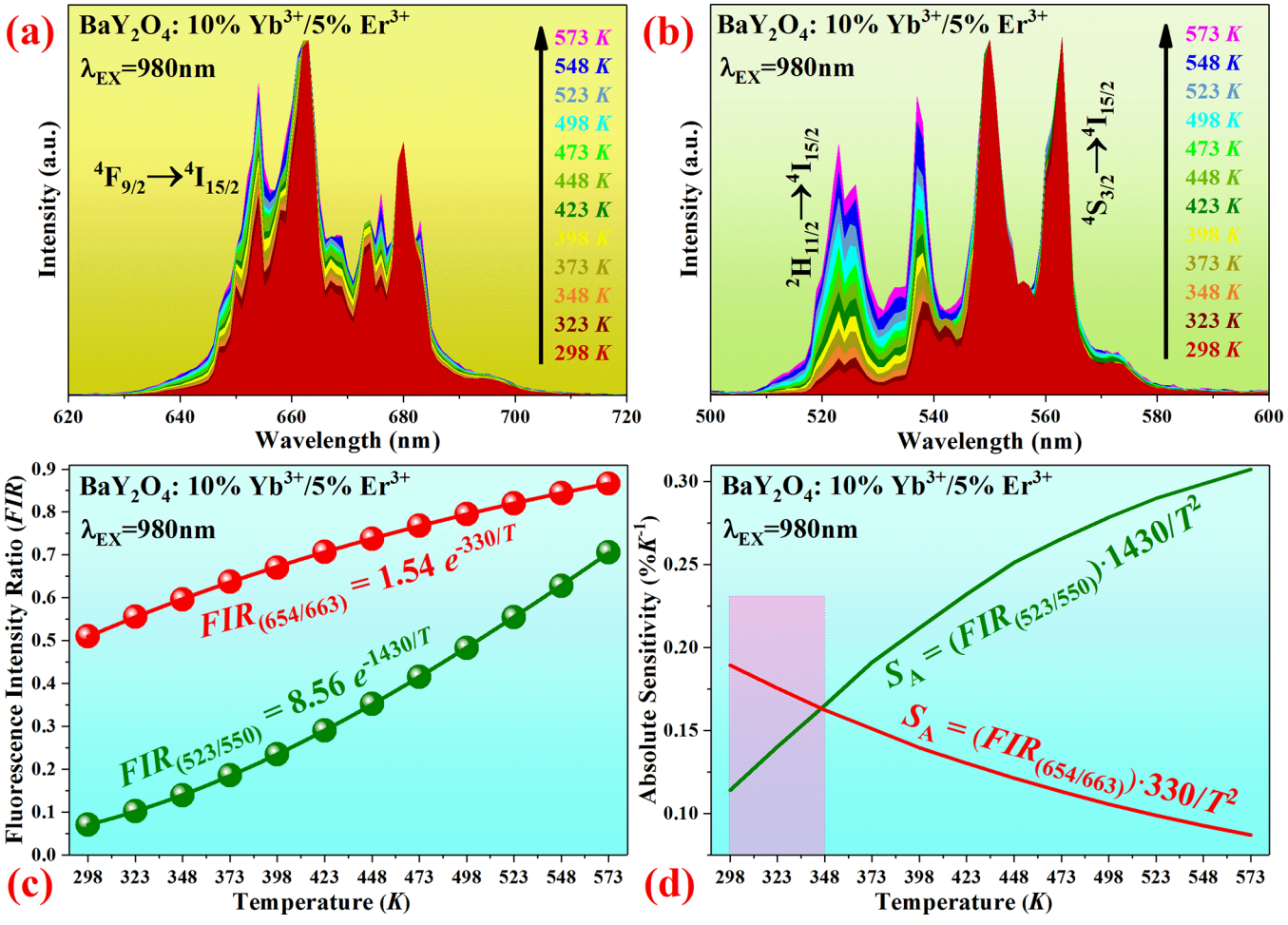

Figure 3. Normalized temperature dependent (a) red UC spectra and (b) green UC spectra. (c) Temperature dependence of the (c) FIR and (d) S_A.

$$\mathrm{FIR} = I_{up}/I_{low} = B \times \exp(-\Delta E/k_B T) \quad (1)$$

Here, I, k_B, and T are the emission intensity, Boltzmann constant and absolute temperature, respectively. B is a constant affirmed by absorption rate, spontaneous emission, and degeneracy degree. Based on the above, the fitting equation for the temperature dependence of $FIR_{(654/663)}$ is achieved and presented in Figure 3c, from which the value of ΔE between

https://dx.doi.org/10.1021/acs.inorgchem.0c01543
Inorg. Chem. 2020, 59, 11054−11060

Table 1. Comparison among several typical TCLs-based optical thermometers operating in the biological windows

host	dopants	transition	wavelength (nm)	working range (K)	$S_{A\text{-max}}$ (% K^{-1})	T_{max} (K)	ref
BaY_2O_4	Yb^{3+}/Er^{3+}	$Er^{3+}:(^4F_{9/2(1)} \rightarrow {}^4I_{15/2})/(^4F_{9/2(2)} \rightarrow {}^4I_{15/2})$	654/663	298−573	0.19	298	this work
$Ba_5Gd_8Zn_4O_{21}$	Yb^{3+}/Er^{3+}	$Er^{3+}:(^4F_{9/2(1)} \rightarrow {}^4I_{15/2})/(^4F_{9/2(2)} \rightarrow {}^4I_{15/2})$	653/674	298−490	0.16	298	43
CaF_2	Nd^{3+}/Y^{3+}	$Nd^{3+}:(^4F_{3/2(1)} \rightarrow {}^4I_{11/2})/(^4F_{3/2(2)} \rightarrow {}^4I_{11/2})$	1041/1062	300−335	0.11	300	46
$NaYF_4$	Nd^{3+}	$Nd^{3+}:(^4F_{7/2} \rightarrow {}^4I_{9/2})/(^4F_{5/2} \rightarrow {}^4I_{9/2})$	740/803	323−500	0.098	500	47
$BaMoO_4$	Yb^{3+}/Er^{3+}	$Er^{3+}:(^4F_{13/2}(Y_i) \rightarrow {}^4I_{15/2}(Z_i))/(^4I_{13/2}(Y_1) \rightarrow {}^4I_{15/2}(Z_1))$	1521/1531	293−553	0.065	293	26
La_2O_2S	Nd^{3+}	$Nd^{3+}:(^4F_{5/2} \rightarrow {}^4I_{9/2})/(^4F_{3/2} \rightarrow {}^4I_{9/2})$	818/897	30−500	0.05	500	48
YF_3	Yb^{3+}/Tm^{3+}	$Tm^{3+}:(^3F_{2,3} \rightarrow {}^3H_6)/(^3H_4 \rightarrow {}^3H_6)$	700/776	310−323	0.034	323	49
$LiNbO_3$	Yb^{3+}/Tm^{3+}	$Tm^{3+}:(^3F_{2,3} \rightarrow {}^3H_6)/(^3H_4 \rightarrow {}^3H_6)$	700/800	323−773	0.033	773	50
La_2O_3	Yb^{3+}/Nd^{3+}	$Nd^{3+}:(^4F_7 \rightarrow {}^4I_{9/2})/(^4F_{5/2} \rightarrow {}^4I_{9/2})$	765/825	293−1233	0.03	693	51
Y_2O_3	Yb^{3+}/Er^{3+}	$Er^{3+}:(^4I_{13/2}(Y_i) \rightarrow {}^4I_{15/2}(Z_i))/(^4I_{13/2}(Y_1) \rightarrow {}^4I_{15/2}(Z_1))$	1574/1533	293−723	0.03	293	52

I_{654} and I_{663} is calculated to be 229 cm^{-1}, close to the value obtained from the corresponding spectra (208 cm^{-1}). Moreover, as an important parameter to qualitatively evaluate the applicability for optical thermometers, the absolute sensitivity S_A of $FIR_{(654/663)}$ is calculated by employing the equation below:

$$S_A = |d(FIR)/dT| = FIR \times (\Delta E/k_B T^2) \quad (2)$$

As illustrated in Figure 3(d), the S_A of $FIR_{(654/663)}$ is monotonously decreased from 0.19 to 0.09% K^{-1} with the rise of temperature from 298 to 573 K. Sequentially, several typical TCLs-based optical thermometers operating in the biological windows are listed in Table 1 to evaluate the thermometric performance of $FIR_{(654/663)}$. Here, we mainly focus on the S_A value of every thermometer, which is a more suitable parameter for the comparison among the same type optical thermometers due to the consideration of FIR value.[53] Clearly, the S_A value of $FIR_{(654/663)}$ shows a greater improvement than the other thermometers operating in the biological windows. More importantly, the groove of $FIR_{(654/663)}$ for thermometry is nicely located in the physiological temperature range as labeled in Figure 3d, indicating its potential thermometry application value in biomedicine.

Beyond that, the temperature sensing behaviors based on the FIR of thermally coupled $^2H_{11/2}$ and $^4S_{3/2}$ are also explored, as shown in parts b−d of Figure 3. In the studied temperature range, the S_A of $FIR_{(523/550)}$ monotonously increases with the rising temperature and reaches its maximum value 0.31% K^{-1} at 573 K. Particularly, the S_A curves of $FIR_{(523/550)}$ and $FIR_{(654/663)}$ intersect at about 348 K, which means that a sensitive thermometry can be realized in a wide temperature range through switching the two thermometers at different temperature. That is to say, for the temperature below 348 K, $FIR_{(654/663)}$ is a reasonable candidate for measuring the temperature because of its relative high sensitivity in this temperature range. Similarly, $FIR_{(523/550)}$ is applicable for high temperature condition (above 348 K). In order to prove this, an infrared thermometer and the FIR technology are simultaneously used to measure the temperature of the sample, which is heated to a certain temperature by a heating gun. Figure 4 shows the measurement results calculated by $FIR_{(523/550)}$ and $FIR_{(654/663)}$ as well as detected by the infrared thermometer. The temperature measured by the infrared thermometer is regarded as the actual temperature. Distinctly, $FIR_{(654/663)}$ and $FIR_{(523/550)}$ show higher accuracy for temperature detection below and above 348 K, respectively. The

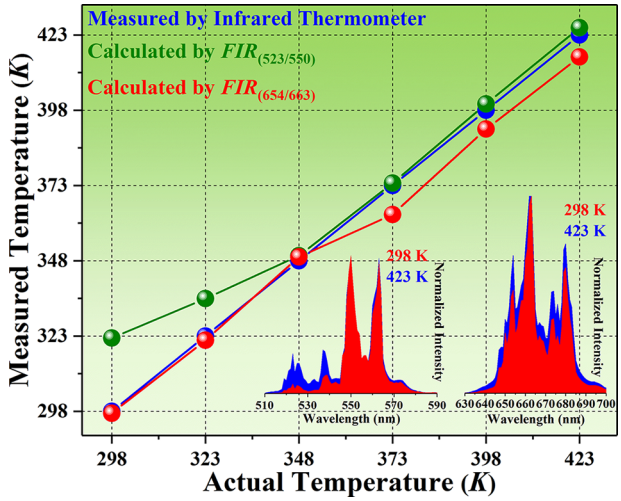

Figure 4. Temperature of the sample determined by $FIR_{(523/550)}$ and $FIR_{(654/663)}$ as well as the infrared thermometer. Inset: the normalized green and red UC spectra detected at 298 and 423 K.

maximum absolute errors for $FIR_{(654/663)}$ and $FIR_{(523/550)}$ in its corresponding working region are 1.4 and 2.4 K, respectively. The repeatability studies of $FIR_{(654/663)}$ and $FIR_{(523/550)}$ in the temperature cycling between 298 and 573 K are shown in Figure S2. Obviously, the values of $FIR_{(654/663)}$ and $FIR_{(523/550)}$ almost keep unchanged during the cycling process, indicating the excellent repeatability and reliability of the present sample.

Ex Vivo Experiments in Biotissues. Penetration depth in the subtissues is a critical parameter of optical thermometer for bioapplication; thus, a simple *ex vivo* experiment is conducted with various fresh chicken breast thickness at room temperature (see Figure S3). As depicted in Figure 5, the luminescence intensity is dramatically decreased with the increasing tissue thickness. Distinctly, the green light signal is completely disappeared under 2-mm-thick tissue. However, the red light can be observed by the naked eye even at a depth of 4 mm. Meanwhile, the spectroscopy signal of the red emission can still be detected below a depth of 6 mm. More importantly, the increasing tissue thickness has almost no influence on the FIR values of I_{654} to I_{663}, as shown in the bar graph. The above results sufficiently demonstrate that the present sample can afford a deep-tissue temperature sensing with high sensitivity.

CONCLUSIONS

In summary, an ultrasensitive temperature sensor operating in the biological window is achieved in $BaY_2O_4:Yb^{3+}/Er^{3+}$,

https://dx.doi.org/10.1021/acs.inorgchem.0c01543
Inorg. Chem. 2020, 59, 11054−11060

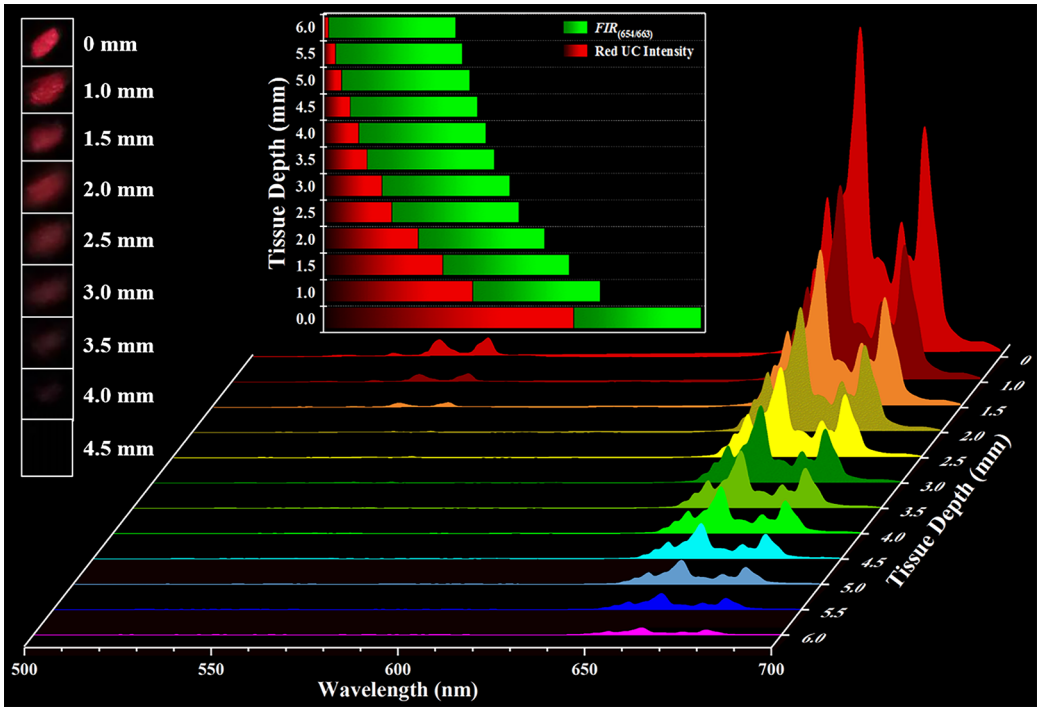

Figure 5. UC spectra of BaY_2O_4:10% Yb^{3+}/5% Er^{3+} with various fresh chicken breast thickness. Inset: tissue thickness dependence of the red UC intensity and FIR as well as the corresponding digital photos.

through the FIR of thermally coupled Stark sublevels of $^4F_{9/2}$. The maximum S_A of $FIR_{(654/663)}$) is 0.19% K^{-1} at 298 K, which is much higher than most previous reports concerning FIR-BW. More importantly, the groove of $FIR_{(654/663)}$ for thermometry is exactly located in the physiological temperature range. Meanwhile, the penetration depth of the red UC emission in biological tissues can reach to 6 mm without any influence on the FIR values of I_{654} to I_{663}. Beyond that, the temperature sensing behaviors of the thermally coupled levels $^2H_{11/2}$ and $^4S_{3/2}$ ($FIR_{(523/550)}$) are also investigated in detail, which can combine with $FIR_{(654/663)}$ to realize a broad scope temperature measurement. In the studied temperature range, the absolute sensitivity of $FIR_{(523/550)}$ monotonously increases with the rising temperature and reaches its maximum value 0.31% K^{-1} at 573 K. All the results declare that the efficient red UC material BaY_2O_4:Yb^{3+}/Er^{3+} is an ultrasensitive temperature probe that can be used for deep-tissue detection.

■ ASSOCIATED CONTENT

Supporting Information

The Supporting Information is available free of charge at https://pubs.acs.org/doi/10.1021/acs.inorgchem.0c01543.

Lorentz fitting of the red UC spectra, repeatability studies of $FIR_{(654/663)}$ and $FIR_{(523/550)}$, scheme of the setup for the *ex vivo* experiment (PDF)

■ AUTHOR INFORMATION

Corresponding Authors

Guotao Xiang − *Department of Mathematics and Physics, Chongqing University of Posts and Telecommunications, Chongqing 400065, China;* orcid.org/0000-0003-3587-6654; Email: xianggt@cqupt.edu.cn

Xiaojun Wang − *Department of Physics & Astronomy, Georgia Southern University, Statesboro, Georgia 30460, United States;* orcid.org/0000-0003-1506-0762; Email: xwang@georgiasouthern.edu

Jiahua Zhang − *State Key Laboratory of Luminescence and Applications, Changchun Institute of Optics, Fine Mechanics and Physics, Chinese Academy of Sciences, Changchun 130033, China*; Email: zhangjh@ciomp.ac.cn

Authors

Xiaotong Liu − *Department of Mathematics and Physics, Chongqing University of Posts and Telecommunications, Chongqing 400065, China*

Qing Xia − *Department of Mathematics and Physics, Chongqing University of Posts and Telecommunications, Chongqing 400065, China*

Sha Jiang − *Department of Mathematics and Physics, Chongqing University of Posts and Telecommunications, Chongqing 400065, China*

Xianju Zhou − *Department of Mathematics and Physics, Chongqing University of Posts and Telecommunications, Chongqing 400065, China;* orcid.org/0000-0002-8050-9688

Li Li − *Department of Mathematics and Physics, Chongqing University of Posts and Telecommunications, Chongqing 400065, China;* orcid.org/0000-0003-1163-5733

Ye Jin − *School of Science, Chongqing University of Technology, Chongqing 400054, China*

Li Ma − *Department of Physics & Astronomy, Georgia Southern University, Statesboro, Georgia 30460, United States*

Complete contact information is available at: https://pubs.acs.org/10.1021/acs.inorgchem.0c01543

Notes

The authors declare no competing financial interest.

https://dx.doi.org/10.1021/acs.inorgchem.0c01543
Inorg. Chem. 2020, 59, 11054−11060

■ ACKNOWLEDGMENTS

This work is financially supported by the National Natural Science Foundation of China (11674044, 11704054), the Chongqing Research Program of Basic Research and Frontier Technology (CSTC2017jcyjAX0046), the Science and Technology Research Program of Chongqing Municipal Education Commission (KJZD-K201800602), and the State Scholarship Fund from the China Scholarship Council (201907845006).

■ REFERENCES

(1) Zhang, Q.; Xu, Y.; Wang, Z.; Zhang, X.; Xia, Z. BiOBr-assisted hydrothermal synthesis of hierarchical $Bi_4(GeO_4)_3/Zn_2GeO_4$ microspheres for optical sensor application. *J. Mater. Chem. C* **2018**, *6* (36), 9778−9785.

(2) Gao, Y.; Cheng, Y.; Hu, T.; Ji, Z.; Lin, H.; Xu, J.; Wang, Y. Broadening the valid temperature range of optical thermometry through dual-mode design. *J. Mater. Chem. C* **2018**, *6* (41), 11178−11183.

(3) Liang, S.; Li, G.; Dang, P.; Wei, Y.; Lian, H.; Lin, J. Cation substitution induced adjustment on lattice structure and photoluminescence properties of $Mg_{14}Ge_5O_{24}:Mn^{4+}$: optimized emission for w-LED and thermometry applications. *Adv. Opt. Mater.* **2019**, *7* (12), 1900093.

(4) Shi, L.; Song, W.; Lian, C.; Chen, W.; Mei, J.; Su, J.; Liu, H.; Tian, H. Dual-emitting dihydrophenazines for highly sensitive and ratiometric thermometry over a wide temperature range. *Adv. Opt. Mater.* **2018**, *6* (15), 1800190.

(5) Chen, Y.; He, J.; Zhang, X.; Rong, M.; Xia, Z.; Wang, J.; Liu, Z. Dual-mode optical thermometry design in $Lu_3Al_5O_{12}:Ce^{3+}/Mn^{4+}$ phosphor. *Inorg. Chem.* **2020**, *59* (2), 1383−1392.

(6) Shang, Y.; Han, Q.; Hao, S.; Chen, T.; Zhu, Y.; Wang, Z.; Yang, C. Dual-mode upconversion nanoprobe enables broad-range thermometry from cryogenic to room temperature. *ACS Appl. Mater. Interfaces* **2019**, *11* (45), 42455−42461.

(7) Trejgis, K.; Bednarkiewicz, A.; Marciniak, L. Engineering excited state absorption based nanothermometry for temperature sensing and imaging. *Nanoscale* **2020**, *12* (7), 4667−4675.

(8) Zhang, H.; Zhao, S.; Wang, X.; Ren, X.; Ye, J.; Huang, L.; Xu, S. The enhanced photoluminescence and temperature sensing performance in rare earth doped $SrMoO_4$ phosphors by aliovalent doping: from material design to device applications. *J. Mater. Chem. C* **2019**, *7* (47), 15007−15013.

(9) Xu, L.; Liu, J.; Pei, L.; Xu, Y.; Xia, Z. Enhanced up-conversion luminescence and optical temperature sensing in graphitic C_3N_4 quantum dots grafted with $BaWO_4:Yb^{3+},Er^{3+}$ phosphors. *J. Mater. Chem. C* **2019**, *7* (20), 6112−6119.

(10) Gao, Y.; Huang, F.; Lin, H.; Zhou, J.; Xu, J.; Wang, Y. A novel optical thermometry strategy based on diverse thermal response from two intervalence charge transfer states. *Adv. Funct. Mater.* **2016**, *26* (18), 3139−3145.

(11) Kaczmarek, A. M.; Kaczmarek, M. K.; Van Deun, R. Er^{3+} to Yb^{3+} and Pr^{3+} to Yb^{3+} energy transfer for highly efficient near-infrared cryogenic optical temperature sensing. *Nanoscale* **2019**, *11* (3), 833−837.

(12) Li, L.; Qi, X.; Qin, F.; Li, L.; Gao, H.; Zheng, Y.; Zhang, Z. Highly sensitive optical ratiometric thermometry by exciting Eu^{3+}/Tb^{3+}'s unusual absorption lines. *Phys. Chem. Chem. Phys.* **2019**, *21* (44), 24308−24315.

(13) Wang, S.; Ma, S.; Zhang, G.; Ye, Z.; Cheng, X. High-performance Pr^{3+}-doped scandate optical thermometry: 200 K of sensing range with relative temperature sensitivity above 2% K^{-1}. *ACS Appl. Mater. Interfaces* **2019**, *11* (45), 42330−42338.

(14) Zhang, J.; Cai, G.; Wang, W.; Ma, L.; Wang, X.; Jin, Z. Tuning of Emission by Eu^{3+} Concentration in a pyrophosphate: the effect of local symmetry. *Inorg. Chem.* **2020**, *59* (4), 2241−2247.

(15) Shi, R.; Ning, L.; Huang, Y.; Tao, Y.; Zheng, L.; Li, Z.; Liang, H. $Li_4SrCa(SiO_4)_2$: Eu^{2+}: a potential temperature sensor with unique optical thermometric properties. *ACS Appl. Mater. Interfaces* **2019**, *11* (10), 9691−9695.

(16) Marciniak, L.; Trejgis, K. Luminescence lifetime thermometry with Mn^{3+}-Mn^{4+} co-doped nanocrystals. *J. Mater. Chem. C* **2018**, *6* (26), 7092−7100.

(17) Ruan, F.; Deng, D.; Wu, M.; Chen, B.; Lei, L.; Lei, R.; Xu, S. Multichannel luminescence properties and ultrahigh-sensitive optical temperature sensing of mixed-valent Eu^{2+}/Eu^{3+} co-activated $Ca_8ZrMg(PO_4)_6(SiO_4)$ phosphors. *J. Alloys Compd.* **2019**, *784*, 1153−1161.

(18) Hou, B.; Jia, M.; Li, P.; Liu, G.; Sun, Z.; Fu, Z. Multifunctional optical thermometry based on the rare-earth-ions-doped up-/down-conversion $Ba_2TiGe_2O_8$: Ln (Ln = $Eu^{3+}/Er^{3+}/Ho^{3+}/Yb^{3+}$) phosphors. *Inorg. Chem.* **2019**, *58* (12), 7939−7946.

(19) Tu, Y.; Zhao, S.; He, D.; Wu, T.; Zhang, H.; Lei, R.; Huang, L.; Xu, S. A portable all-fiber thermometer based on the fluorescence intensity ratio (FIR) technique in rare earth doped TeO_2-WO_3-La_2O_3-Na_2O glass. *J. Mater. Chem. C* **2018**, *6* (26), 7063−7069.

(20) Back, M.; Ueda, J.; Xu, J.; Murata, D.; Brik, M. G.; Tanabe, S. Ratiometric luminescent thermometers with a customized phase-transition-driven fingerprint in perovskite oxides. *ACS Appl. Mater. Interfaces* **2019**, *11* (42), 38937−38945.

(21) Kolesnikov, I. E.; Kalinichev, A. A.; Kurochkin, M. A.; Mamonova, D. V.; Kolesnikov, E. Y.; Lahderanta, E. Ratiometric optical thermometry based on emission and excitation spectra of YVO_4: Eu^{3+} nanophosphors. *J. Phys. Chem. C* **2019**, *123* (8), 5136−5143.

(22) Li, L.; Tang, X.; Wu, Z.; Zheng, Y.; Jiang, S.; Tang, X.; Xiang, G.; Zhou, X. Simultaneously tuning emission color and realizing optical thermometry via efficient $Tb^{3+}\rightarrow Eu^{3+}$ energy transfer in whitlockite-type phosphate multifunctional phosphors. *J. Alloys Compd.* **2019**, *780*, 266−275.

(23) Ptak, M.; Dziuk, B.; Stefanska, D.; Hermanowicz, K. The structural, phonon and optical properties of $[CH_3NH_3]$-$M_{0.5}Cr_xAl_{0.5-x}(HCOO)_3$ (M = Na, K; x = 0, 0.025, 0.5) metal-organic framework perovskites for luminescence thermometry. *Phys. Chem. Chem. Phys.* **2019**, *21* (15), 7965−7972.

(24) Zareba, J. K.; Nyk, M.; Janczak, J.; Samoc, M. Three-photon absorption of coordination polymer transforms UV-to-VIS thermometry into NIR-to-VIS thermometry. *ACS Appl. Mater. Interfaces* **2019**, *11* (11), 10435−10441.

(25) Liu, S.; Cui, J.; Jia, J.; Fu, J.; You, W.; Zeng, Q.; Yang, Y.; Ye, X. High sensitive Ln^{3+}/Tm^{3+} /Yb^{3+} (Ln^{3+} = Ho^{3+}, Er^{3+}) tri-doped $Ba_3Y_4O_9$ upconverting optical thermometric materials based on diverse thermal response from non-thermally coupled energy levels. *Ceram. Int.* **2019**, *45* (1), 1−10.

(26) Lei, R.; Liu, X.; Huang, F.; Deng, D.; Zhao, S.; Xu, H.; Xu, S. Optical thermometry based on anomalous temperature-dependent 1.53 μm infrared luminescence of Er^{3+} in $BaMoO_4$: Er^{3+}/Yb^{3+} phosphor. *Opt. Mater.* **2018**, *86*, 278−285.

(27) Zhang, H.; Ye, J.; Wang, X.; Zhao, S.; Lei, R.; Huang, L.; Xu, S. Highly reliable all-fiber temperature sensor based on the fluorescence intensity ratio (FIR) technique in Er^{3+}/Yb^{3+} co-doped $NaYF_4$ phosphors. *J. Mater. Chem. C* **2019**, *7* (48), 15269−15275.

(28) Zhao, Z.; Li, K.; Liu, C.; Yin, Q.; Han, J.; Heo, J. Intense up-conversion emission from Er^{3+}/Yb^{3+} ion co-doped transparent oxyfluoride glass-ceramics containing $Y_5O_4F_7$ nanorods for optical thermometry. *J. Mater. Chem. C* **2019**, *7* (20), 6134−6143.

(29) Suo, H.; Zhao, X.; Zhang, Z.; Shi, R.; Wu, Y.; Xiang, J.; Guo, C. Local symmetric distortion boosted photon up-conversion and thermometric sensitivity in lanthanum oxide nanospheres. *Nanoscale* **2018**, *10* (19), 9245−9251.

(30) Xiang, G.; Liu, X.; Liu, W.; Wang, B.; Liu, Z.; Jiang, S.; Zhou, X.; Li, L.; Jin, Y.; Zhang, J. Multifunctional optical thermometry based on the stark sublevels of Er^{3+} in $CaO-Y_2O_3:Yb^{3+}/Er^{-3+}$. *J. Am. Ceram. Soc.* **2020**, *103* (4), 2540−2547.

(31) Li, L.; Qin, F.; Li, L.; Gao, H.; Zhang, Z. New strategy for circumventing the limitation of thermally linked states and boosting

https://dx.doi.org/10.1021/acs.inorgchem.0c01543
Inorg. Chem. 2020, 59, 11054−11060

the relative thermal sensitivity of luminescence ratiometric thermometry. *J. Phys. Chem. C* **2019**, *123* (10), 6176−6181.
(32) Wu, Y.; Lai, F.; Liu, B.; Huang, J.; Ye, X.; You, W. Sensitivity improvement induced by thermal response behavior for temperature sensing applications. *Phys. Chem. Chem. Phys.* **2019**, *21* (29), 16316−16322.
(33) Gutierrez-Cano, V.; Rodriguez, F.; Gonzalez, J. A.; Valiente, R. Upconversion and optical nanothermometry in $LaGdO_3$: Er^{3+} nanocrystals in the RT to 900 K range. *J. Phys. Chem. C* **2019**, *123* (49), 29818−29828.
(34) Fischer, L. H.; Harms, G. S.; Wolfbeis, O. S. Upconverting nanoparticles for nanoscale thermometry. *Angew. Chem., Int. Ed.* **2011**, *50* (20), 4546−4551.
(35) Singh, S. K.; Kumar, K.; Rai, S. B. Er^{3+}/Yb^{3+} codoped Gd_2O_3 nano-phosphor for optical thermometry. *Sens. Actuators, A* **2009**, *149* (1), 16−20.
(36) Liu, K. C.; Zhang, Z. Y.; Shan, C. X.; Feng, Z. Q.; Li, J. S.; Song, C. L.; Bao, Y. N.; Qi, X. H.; Dong, B. A flexible and superhydrophobic upconversion-luminescence membrane as an ultrasensitive fluorescence sensor for single droplet detection. *Light: Sci. Appl.* **2016**, *5* (8), No. e16136.
(37) Wang, F.; Wen, S.; He, H.; Wang, B.; Zhou, Z.; Shimoni, O.; Jin, D. Microscopic inspection and tracking of single upconversion nanoparticles in living cells. *Light: Sci. Appl.* **2018**, *7* (4), 18007.
(38) Qin, W. P.; Liu, Z. Y.; Sin, C. N.; Wu, C. F.; Qin, G. S.; Chen, Z.; Zheng, K. Z. Multi-ion cooperative processes in Yb^{3+} clusters. *Light: Sci. Appl.* **2014**, *3* (8), No. e193.
(39) Zhang, J.; Hao, Z.; Li, J.; Zhang, X.; Luo, Y.; Pan, G. Observation of efficient population of the red-emitting state from the green state by non-multiphonon relaxation in the Er^{3+}-Yb^{3+} system. *Light: Sci. Appl.* **2015**, *4* (1), No. e239.
(40) Suo, H.; Zhao, X.; Zhang, Z.; Li, T.; Goldys, E. M.; Guo, C. Constructing multiform morphologies of YF: Er^{3+}/Yb^{3+} upconversion nano/micro-crystals towards sub-tissue thermometry. *Chem. Eng. J.* **2017**, *313*, 65−73.
(41) Zhang, Z.; Guo, C.; Suo, H.; Zhao, X.; Zhang, N.; Li, T. Thermometry and up-conversion luminescence of Yb^{3+}-Er^{3+} co-doped $Na_2Ln_2Ti_3O_{10}$ (Ln = Gd, La) phosphors. *Phys. Chem. Chem. Phys.* **2016**, *18* (28), 18828−18834.
(42) Hong, G.; Antaris, A.; Dai, H. Near-infrared fluorophores for biomedical imaging. *Nat. Biomed. Eng.* **2017**, *1* (1), 1−22.
(43) Suo, H.; Guo, C.; Li, T. Broad-Scope Thermometry based on dual-color modulation up-conversion phosphor $Ba_5Gd_8Zn_4O_{21}$:Er^{3+}/Yb^{3+}. *J. Phys. Chem. C* **2016**, *120* (5), 2914−2924.
(44) Runowski, M.; Stopikowska, N.; Szeremeta, D.; Goderski, S.; Skwierczynska, M.; Lis, S. Upconverting lanthanide fluoride core@shell nanorods for luminescent thermometry in the first and second biological windows: beta-$NaYF_4$:Yb^{3+}-Er^{3+}@SiO_2 temperature sensor. *ACS Appl. Mater. Interfaces* **2019**, *11* (14), 13389−13396.
(45) Wu, H.; Hao, Z.; Zhang, L.; Zhang, X.; Xiao, Y.; Pan, G. H.; Wu, H.; Luo, Y.; Zhang, L.; Zhang, J. Er^{3+}/Yb^{3+} codoped phosphor $Ba_3Y_4O_9$ with intense red upconversion emission and optical temperature sensing behavior. *J. Mater. Chem. C* **2018**, *6* (13), 3459−3467.
(46) Quintanilla, M.; Zhang, Y.; Liz-Marzan, L. M. Subtissue Plasmonic Heating Monitored with CaF_2: Nd^{3+}, Y^{3+} Nanothermometers in the Second Biological Window. *Chem. Mater.* **2018**, *30* (8), 2819−2828.
(47) Tian, X.; Wei, X.; Chen, Y.; Duan, C.; Yin, M. Temperature sensor based on ladder-level assisted thermal coupling and thermal-enhanced luminescence in $NaYF_4$: Nd^{3+}. *Opt. Express* **2014**, *22* (24), 30333−30345.
(48) Jiang, G.; Wei, X.; Zhou, S.; Chen, Y.; Duan, C.; Yin, M. Neodymium doped lanthanum oxysulfide as optical temperature sensors. *J. Lumin.* **2014**, *152*, 156−159.
(49) Suo, H.; Hu, F.; Zhao, X.; Zhang, Z.; Li, T.; Duan, C.; Yin, M.; Guo, C. All-in-one thermometer-heater up-converting platform YF_3:Yb^{3+}, Tm^{3+} operating in the first biological window. *J. Mater. Chem. C* **2017**, *5* (6), 1501−1507.
(50) Xing, L.; Yang, W.; Ma, D.; Wang, R. Effect of crystallinity on the optical thermometry sensitivity of Tm^{3+}/Yb^{3+} codoped $LiNbO_3$ crystal. *Sens. Actuators, B* **2015**, *221*, 458−462.
(51) Gao, G.; Busko, D.; Kauffmann-Weiss, S.; Turshatov, A.; Howard, I. A.; Richards, B. S. Wide-range non-contact fluorescence intensity ratio thermometer based on Yb^{3+}/Nd^{3+} co-doped La_2O_3 microcrystals operating from 290 to 1230 K. *J. Mater. Chem. C* **2018**, *6* (15), 4163−4170.
(52) Rakov, N.; Maciel, G. S. Exploring the $^4I_{13/2} \rightarrow {}^4I_{15/2}$ radiative transition from Er^{3+} in Y_2O_3 for temperature sensing. *J. Lumin.* **2018**, *199*, 293−297.
(53) Suo, H.; Zhao, X.; Zhang, Z.; Guo, C. Ultra-sensitive optical nano-thermometer $LaPO_4$:Yb^{3+}/Nd^{3+} based on thermo-enhanced NIR-to-NIR emissions. *Chem. Eng. J.* **2020**, *389*, 124506.

https://dx.doi.org/10.1021/acs.inorgchem.0c01543
Inorg. Chem. 2020, 59, 11054−11060